A comprehensive evaluation of the thermal neutron detection efficiency by a single crystal CVD diamond detector with a LiF thermal neutron converter

Makoto I. Kobayashi[1,2], Sachiko Yoshihashi[3], Kunihiro Ogawa[1,2], Mitsutaka Isobe[1,2], Siriyaporn Sangaroon[1,4], Shuji Kamio[1], Yutaka Fujiwara[1], Masaki Osakabe[1,2]

1. National Institute for Fusion Science, National Institutes of Natural Sciences
2. The Graduate University for Advanced Studies, SOKENDAI
3. Nagoya University
4. Mahasarakham University

Abstract

Thermal neutron detection efficiency of the single crystal CVD diamond detector (SDD) equipping 1.9 μm-thick ^{6}LiF thermal neutron converter, which induces the energetic ions through the ^{6}Li(n,α)^{3}H reaction, was evaluated comprehensively using a charge-integral based pulse shape discrimination (PSD) method and radiation transport calculation by PHITS. The PSD method applied in this work successfully separated the pulses induced by energetic tritons, alpha particles and other types of radiation. The detection efficiency of tritons was consistent with the radiation transport calculation, although that of alpha particles was lower than the estimation. The overall thermal neutron detection efficiency was obtained by summing detection efficiencies of tritons and alpha particles. Approximately 29% of ^{6}Li(n,α)^{3}H reaction occurred in an effective 1.9 μm-thick ^{6}LiF thermal neutron converter could be detectable as the pulses of tritons (~ 73%) and alpha particles (23%).

Keyword: diamond detector, neutron, pulse shape discrimination, PHITS

1. Introduction

A single crystal diamond (SCD) has been considered for the application on a fast neutron detector based on the elastic collision and (n,α) reactions of fast neutron with constituent carbon atoms [1-4]. The characteristics of SCD such as high radiation tolerance, small size, and high temperature tolerance are suitable for the deuterium (D)-tritium (T) fusion reactor environment [5-6]. A single crystal diamond detector (SDD) consists of a SCD with the electrode contact on both surfaces. Applying a voltage on a side of the electrode of the SCD (besides, another surface electrode is grounded), the hole-electron (h-e) pairs generated in the SCD by radiations drift to the electrodes by the electric field, providing the radiation detection according to Schockley-Ramo theorem [7-8].

Also, a foil of lithium or boron placed on the SCD can function as a thermal neutron converter to provide the energetic ions by the (n,α) reaction with thermal neutrons [9-11]. The energy deposition of energetic ions from the thermal neutron converter into the SCD gives a signal in the SDD. Therefore, thermal neutron detection is also possible by the SDD in this manner. According to this additional capability for thermal neutron detection as well as the above-mentioned advantages such as high temperature and radiation tolerances, the SDD has been regarded as a promising detector for evaluating the thermal neutron flux in the blanket in which fuel tritium is generated mainly by $^{6}Li(n,\alpha)^{3}H$ reaction. For this application, one of the important issues is to develop the method to discriminate the signals between gamma-rays and energetic ions because neutrons always associate with gamma-rays. In our previous study, the discrimination of signals induced by energetic ions and gamma-rays was demonstrated based upon the difference in the pulse-width originating from the distribution of h-e pairs induced by the two radiations above [12]. The thermal neutron was detected using a ^{6}Li enriched lithium fluoride (^{6}LiF) foil, which produces the energetic triton and alpha particles, near the SCD. The signals of energetic ions were successfully separated from those induced by gamma-rays using the PSD (pulse shape discrimination) method. On the other hand, the precise evaluation of the detection efficiency for thermal neutrons by the SDD is not completed yet. Because of the asymmetric structure of the SDD equipping one thermal neutron converter, the thermal neutron detection efficiency can vary by the neutron direction. Therefore, a thermal neutron beam injection into the SDD under a low gamma-ray flux environment was carried out in this study to evaluate the thermal neutron detection efficiency precisely. Also, the influence of beam direction on the thermal neutron detection efficiency was investigated. The signal of the energetic ions induced by the thermal neutrons was separately measured by a newly developed PSD method based on the charge-integral of a pulse. The thermal neutron detection efficiency evaluated in this work was compared to the radiation transport model for the overall evaluation of the measurement and the analysis applied in this work.

2. Pulse shape discrimination

As mentioned above, the PSD method should be applied for quantifying energetic ions induced by

the $^{6}Li(n,\alpha)^{3}H$ reaction because the SCD is also sensitive for gamma-rays. Our previous study indicated that the pulse shapes in the SDD induced by energetic ions and gamma-rays were different [12]. In the case of energetic ion injection, the rectangular-shaped pulse was obtained [13-14]. On the other hand, the triangular-shaped pulse was obtained by gamma-ray irradiations. The previous version of the PSD method employed the pulse-width for emphasizing this difference in the pulse shape. However, this method was significantly influenced by the fluctuation of the signal in the process to evaluate the pulse-width. In this study, the charge-integral method was adopted which has advantages such as fast processing and stability for fluctuation of signal

In this method, first, all current data points in a single pulse event, which consisted of 64 data points for 64 ns in total, were subtracted by the background current. Then, all current data points were integrated with respect to time. The integrated current in the short time duration from the beginning of the pulse was defined as Q_{fast}. The integrated current for an entire pulse was defined as Q_{total}. The definitions of Q_{fast} and Q_{total} can be found in Fig. 1 where a pulse by an alpha particle is displayed as an example. In the case of gamma-ray irradiations, the current quickly decreased after the peak-top although the current remained constant for a certain duration in the case of energetic ion irradiations. Accordingly, the ratio of Q_{fast} to Q_{total} (Q_{fast}/Q_{total}) for the pulse induced by a gamma-ray should be larger than that for the pulse induced by an energetic ion. In this study, the duration of 5 ns was employed for evaluating Q_{fast}.

For finding the beginning time of a pulse, the following algorithm was adopted.

$$\boldsymbol{t_{start}} = argmin\left[\left(\boldsymbol{a_j} - a_{th}\right) \times \left(\boldsymbol{a_{j+1}} - a_{th}\right)\right],\ (j = 1 \sim \boldsymbol{t_{Peak}}),$$

where t_{start} is a beginning time of a pulse in each event, t_{peak} is a peak-top time, a is current data after background current subtraction, and a_{th} is a threshold current. Note that t_{start}, t_{peak} and a are different in each pulse event, and a constant a_{th} was applied in this work. This equation indicates that the current data with the subtraction by the threshold current before the beginning of a pulse should be less than zero when sufficiently high threshold current is set. Therefore, the value of $\left(\boldsymbol{a_j} - a_{th}\right) \times \left(\boldsymbol{a_{j+1}} - a_{th}\right)$ is positive there. At the beginning of the pulse, the values of $\left(\boldsymbol{a_j} - a_{th}\right)$ and $\left(\boldsymbol{a_{j+1}} - a_{th}\right)$ are negative and positive, respectively. Therefore, the product of these terms is negative. The product of these terms is positive during the pulse. Therefore, the first position where the product of $\left(\boldsymbol{a_j} - a_{th}\right)$ and $\left(\boldsymbol{a_{j+1}} - a_{th}\right)$ is negative is the beginning time of the pulse.

The PSD method applied in this study was demonstrated using an alpha particle source and a gamma-ray source. As an alpha particle source, ^{241}Am was used, which emits alpha particles with the energy of ~ 5.5 MeV [15]. As a gamma-ray source, ^{60}Co was used. The energies of gamma-rays from ^{60}Co are 1.173 and 1.333 MeV [15]. The PSD results using the above two radiation sources are displayed in Fig. 2. The count rates and total numbers of pulses for alpha particles and gamma-rays were 19 cps and 30 cps, and ~24000 (measurement for 1200s) and ~110000 (measurement for 3600 s), respectively.

There were two regions of pulse group with higher Q_{total} and lower Q_{tatal}, which should be assigned to the pulses induced by alpha particles from ^{241}Am and gamma-rays from ^{60}Co, respectively. The values of Q_{fast}/Q_{total} were scattered for the pulses by gamma-rays compared to those by alpha particles. This difference in the distribution of Q_{fast}/Q_{total} should be caused by the difference in the production position of h-e pairs in the SCD by alpha particles and gamma-rays. 5.5 MeV alpha particles deposited all energy into the surface region of the SCD. On the other hand, the energy deposition by gamma-rays occurred at random positions in the entire bulk of the SCD. This leads to various distributions of h-e pairs in the SCD in each gamma-ray event, resulting in the different Q_{fast}/Q_{total}. Another reason should be the low Q_{total} in gamma-ray irradiations. Gamma-ray energy deposition in the SCD is dominated by Compton scattering. Therefore, gamma-rays interacting with the SCD deposit only part of their energy. Such a low energy pulse has a low pulse height, therefore, the pulses induced by gamma-rays were usually influenced by the oversubtraction in the background subtraction process. This oversubtraction raised the baseline level, leading to the scattering of Q_{fast}/Q_{total}. In any case, Fig. 2 demonstrated that the discrimination of pulses induced by alpha particles and gamma-rays using Q_{fast}/Q_{total} was achievable. In this study, the PSD method explained in this section was used in the following experiments.

3. Experimental

3.1 Single crystal CVD diamond detector

The SDD (B6-C compact thermal-neutron diamond detector) manufactured by Cividec instrumentation GmbH was used in this work [16]. The SCD was a single crystal, electronic grade, chemical vapor deposition diamond. The size of the SCD was 4.5 mm × 4.5 mm, and the thickness was 500 μm. A 100 nm-thick titanium layer was deposited on both SCD surfaces to work as the electrodes. The detector housing had the size of 54 × 10 × 5.5 mm^3, and was composed by polyether ether ketone (PEEK). This detector equipped the ^{6}Li-enriched LiF (^{6}LiF) thermal neutron converter with the thickness of 1.9 μm. The isotopic abundance of ^{6}Li in this layer was 95%. The energetic ions of triton and alpha particles are generated by ^{6}Li(n,α)^{3}H reaction with thermal neutrons. The recoil energy of triton and alpha particles are about 2.7 MeV and 2.0 MeV, respectively. The energetic ions should deposit their energies into the SCD through the window with a diameter of 3.6 mm$^{\varphi}$. The distance between the SCD and the ^{6}LiF layer was 1.0 mm. The details of the structure of SDD can be found in Fig. 3.

The signal produced by the SDD was sent to a pre-amplifier (C2-HV broadband amplifier of CIVIDEC). The amplified signal was recorded by the DAQ system (APV8102-14MWPSAGb) composed of fast processing ADC and FPGA system with the sampling rate of 1 GHz and the resolution of 14 bit. The details of the data acquisition system used in this work can be found elsewhere [17].

3.2 Thermal neutron irradiation

For the precise evaluation of the thermal neutron detection efficiency, the E-3 port of the Kyoto University Reactor (KUR) was used in this study. In this port, thermal neutrons from KUR were guided through the wall of the KUR torus hall to decrease the gamma-ray dose. Then, the thermal neutron beam passed the collimator with the size of 15 × 20 mm^2 located at 750 mm from the port. The irradiation position was located at 600 mm from the collimator. Before the irradiation, the thermal neutron flux was evaluated as 2.7×10^5 n cm^{-2} s^{-1} by the activation foil method using gold. Then, the thermal neutron measurement was carried out by inserting the detector into the beam line. The thick LiF sheet was placed on the backside of the detector to absorb all thermal neutrons which did not react with the detector to mitigate the influence of scattered neutrons in the experiment.

In this study, two irradiation setups were used. In Case I, the thermal neutron beam was injected into the normal surface of the SCD in the SDD through the ^{6}LiF foil. In Case II, the thermal neutron beam penetrated through the housing of the SDD into the SCD, and then was injected into the ^{6}LiF foil. The irradiation directions in these two cases can be found in Fig. 3.

4. Radiation transport calculation

The thermal neutron detection efficiency of the SDD was also evaluated through radiation transport calculations using PHITS (Particle and Heavy Ion Transport code System) [18]. The geometry of the SDD was precisely modeled as shown in Fig. 3. A plane neutron source with the size of 4.5 mm × 4.5 mm (comparable to the size of the SCD) was placed to emit thermal neutrons with the energy of 0.025 eV. The directions of the thermal neutron beams were opposite in Cases I and II, and the beam injection angles in both cases were perpendicular to the SCD normal. Then, the radiation transport behaviors including the neutron transport, the generation of energetic ions in the ^{6}LiF foil, the transport of energetic ions, and the energy deposition in the SCD in Cases I and II were evaluated. The count number as a function of deposited energy into the SCD in a single event was estimated by T-deposit tally. The trigger level was imitated using the energy cut-off of 300 keV for energetic ions.

5. Results and discussion

The results of PSD applied for approximately 53000 pulse data obtained by the thermal neutron irradiations for 9 min in Case I are displayed in Fig. 4. The event rate in this measurement was around 98 s^{-1}. In the PSD results, there were three regions. The first region was located in $2000 < Q_{total} < 2800$ and $0.30 < Q_{fast}/Q_{total} < 0.46$. The second region was in $900 < Q_{total} < 1500$ and $0.32 < Q_{fast}/Q_{total} < 0.50$. The third region placed with similar Q_{total} to the second region, although Q_{fast}/Q_{total} was much larger. A lower Q_{fast}/Q_{total} of the first region should indicate that this pulse group was induced by energetic ions. Here, Q_{total} in the first region corresponded to 2.0-2.9 MeV according to Q_{total} of alpha

particles from ^{241}Am as shown in Fig. 2. Therefore, the first region was assigned to the energetic tritons generated by the ^{6}Li(n,α)^{3}H reaction. The range of Q_{fast}/Q_{total} for the second region suggested that this pulse group was also induced by energetic ions. Therefore, the pulse group in the second region was assigned to alpha particles induced by the ^{6}Li(n,α)^{3}H reaction with the recoil energy of 2.0 MeV. On the other hand, the Q_{total} of the second region corresponded to 0.9-1.5 MeV, which was significantly lower than the recoil energy of alpha particles by the ^{6}Li(n,α)^{3}H reaction. The third region showed higher Q_{fast}/Q_{total}, and Q_{total} was comparable to or lower than that of the second region. According to these facts, the pulse group in the third region would be caused by the Compton scattering of gamma-rays or the elastic collision of neutrons, which can induce the low energy deposition into the bulk of the SCD.

The transport behaviors of thermal neutrons and the energetic tritons in Case I estimated by PHITS are depicted in Fig. 5(a) and 5(b), respectively. In these figures, the thermal neutron beam enters the SDD from the right side to the left side. Most of the thermal neutrons passed through the SDD, although the flux of thermal neutrons decreased after passing through the SDD. Part of the thermal neutrons collided with the constituent atoms of the SDD, and thermal neutron scattering can be observed. For the case of triton transport, the flux of energetic tritons can be observed only in the region between the ^{6}LiF foil and the SCD because energetic tritons transported to the opposite direction from the SCD immediately stopped by the housing of the SDD. The flux was high on the surface of the ^{6}LiF and decreased in the region near the side wall of the window, forming a concentric distribution. The transport behavior of alpha particles was similar to tritons, although the flux was lower. The results for Case II were similar to those for Case I (not shown here). The thermal neutron flux in the ^{6}LiF foil in Case II decreased compared to Case I because thermal neutrons must pass through a longer distance in the housing of the SDD. Accordingly, the flux of energetic tritons was also lower in Case II compared to Case I.

The histogram of Q_{total} which corresponds to the deposited energy into the SCD measured in Case I was summarized and is displayed in Fig. 6(a). The bin-size of this histogram is approxmately 70 keV. Also, histograms of Q_{total} of tritons and alpha particles (the pulse groups as first and second regions in Fig. 4, respectively) are added in this figure. The unit of Q_{total} is calibrated to MeV, according to the Q_{total} of alpha particles from ^{241}Am as shown in Fig. 2. The histogram of Q_{total} showed two peaks. The profile of the histogram was quite different from that observed in our previous study where the first peak was dominant [12]. In the previous study, the ^{252}Cf spontaneous fission neutron source was used where influence of gamma-rays from the source was significant. A low gamma-ray flux environment was achieved in this study, and it was suitable for evaluating the thermal neutron detection efficiency. The PSD results indicated that the pulses with high Q_{total} above 2 MeV was caused by tritons. On the other hand, the pulse by alpha particles could be discriminated from the other pulses with the similar Q_{total} by the PSD method. The expected histograms of deposited energy by tritons and alpha particles

during thermal neutron irradiation in Case I by PHITS are also displayed in Fig. 6(b). The bin-size of this histogram is 36 keV. The profiles of these histograms were almost similar to the experimental data with PSD processing. However, the peak-top energy of the expected histogram of alpha particles was at the higher energy side compared to the Q_{total} of the alpha particles induced pulses in this measurement.

Table 1 summarizes the detection efficiencies of energetic ions in Cases I and II obtained in this work. Those estimated by PHITS are also presented in this table. The detection efficiency of alpha particles was almost one-third compared to that of tritons, as observed in the Q_{total} histogram. The detection efficiencies in Case II were lower than those in Case I. The thermal neutron transport calculation by PHITS presented in Fig. 5 showed the scattering of thermal neutrons in the SDD. This fact suggests that the amount of scattered thermal neutrons before reaching ^{6}LiF was larger in Case II than that in Case I because thermal neutrons needed to penetrate thicker SDD housing and the SCD. The ratio of the detection efficiency estimated by the calculation (C) to that evaluated by the experiment (E) was almost consistent for tritons in both Cases I and II. However, C/E for alpha particles in both Cases I and II were larger than unity. The possible reason for the lower detection efficiency of alpha particles in the actual measurement would be due to the lower pulse-height induced by slowed-down alpha particles injection in the SDD. The pulse data including 64 data points were firstly subtracted by the background current signal. A slightly high background signal would induce the oversubtraction of the pulse height, resulting in the lowered Q_{total} of a pulse. This influence should be significant in a low energy pulse induced by slowed-down alpha particles compared to tritons. Actually, the Q_{total} of pulses by alpha particles presented in Fig. 6(a) was lower than that estimated by PHITS due to the influence of the oversubtraction. Therefore, the detection efficiency decreased for alpha particles measurement because a part of alpha particle induced pulses with a lowered pulse-height could not exceed the trigger level of measurement.

As the results of detection efficiency evaluation, we obtained the thermal neutron detection efficiencies by summing those of tritons and alpha particles as $(2.9 \pm 0.1) \times 10^{-4}$ count/(n cm^{-2}) for Case I and $(2.1 \pm 0.1) \times 10^{-4}$ count/(n cm^{-2}) for Case II. These values of the detection efficiency indicate that approximately 29% of energetic ions generated by the ^{6}Li(n,α)^{3}H reaction in 3.6 mm$^{\varphi}$ sized ^{6}LiF (an effective window size for energetic ions in the SDD as shown in Fig. 3) can be detectable as the pulses by tritons (~ 73%) and alpha particles (23%).

6. Conclusion

The PSD method based on the simple charge-integral calculation successfully separated the pulses induced by energetic tritons, alpha particles and other types of radiation. The overall thermal neutron detection efficiencies were evaluated by summing detection efficiencies of tritons and alpha particles as $(2.9 \pm 0.1) \times 10^{-4}$ count/(n cm^{-2}) for Case I and $(2.1 \pm 0.1) \times 10^{-4}$ count/(n cm^{-2}) for Case II. Neutrons

are scattered and thermalized in the blanket of fusion reactors. In such condition, the detection efficiency should be $(2.5\pm0.2) \times 10^{-4}$ count/(n cm^{-2}), which was deduced as an average of the detection efficiencies evaluated in Cases I and II. The neutronics experiments to evaluate the thermal neutron flux distribution in the blanket mock-up are planned and to be conducted using the detection efficiency obtained in this work.

Acknowledgments

This work is supported by the NINS program for cross-disciplinary study (Grant Number 0131190). This work is also performed with the support and under the auspices of the NIFS Collaboration Research program (NIFS19KOAA001, NIFS19KLPA001), and LHD project budget. This work has been performed by using facilities of the Institute for Integrated Radiation and Nuclear Science, Kyoto University.

References

[1]. B. Wolle, Tokamak plasma diagnostics based on measured neutron signals, Phys. Reports, 312 (1999) 1-86.

[2]. O.N. Jarvis, Neutron measurement techniques for tokamak plasmas, Plasma Phys. Control. Fusion, 36 (1994) 209-244.

[3]. M. Sasao et al., Fusion product diagnostics, Fusion Sci. Technol., 53 (2008) 604-639.

[4]. M. Pillon et al., Experimental response functions of a single-crystal diamond detector for 5-20.5 MeV neutrons, Nucl. Instru. Meth. In phys. Res. A640 (2011) 185.

[5]. D. Rigamonti, L. Giacomelli, G. Gorini, M. Nocente, M. Rebai, M. Tardocchi et al., Neutron spectroscopy measurements of 14 MeV neutrons at unprecedented energy resolution and implications for deuterium-tritium fusion plasma diagnostics, Meas. Sci. Technol. 29 (2018) 045502.

[6]. A. Muraro, L. Giacomelli, M. Nocente, M. Rebai, D. Rigamonti, F. Belli et al., First neutron spectroscopy measurements with a pixelated diamond detector at JET, Rev. Sci. Instrum. 87 (2016) 11D833.

[7]. W. Shockley, Currents to Conductors Induced by a Moving Point Charge, J. Appl. Phys. 9 (1938) 635-636.

[8]. Zhong He, Review of the Shockley–Ramo theorem and its application in semiconductor gamma-ray detectors, Nucl. Instrum. Methods Phys. Res. A, 463 (2001) 250-267.

[9]. Makoto Kobayashi, Kunihiro Ogawa, Mitsutaka Isobe, Takeo Nishitani, Shuji Kamio, Yutaka Fujiwara, Tomomi Tsubouchi, Sachiko Yoshihashi, Akira Uritani, Minoru Sakama, Masaki

Osakabe and the LHD Experiment Group, Thermal neutron flux evaluation by a single crystal CVD diamond detector in LHD deuterium experiment, J. Instrum., 14 (2019) C09039.

[10]. M. Pillon, et. al, Development of on-line tritium monitor based upon artificial diamond for fusion applications, IEEE Trans. Nucl. Sci. vol. 58 n.3 (2011) 1141.

[11]. M. Angelone, N. Fonnesu, A. Colangeli, F. Moro, M. Pillon, R. Villari, Calibration and test of a 6LiF-diamond detector for the HCPB mock-up experiment at JET, Fus. Eng. Des. 146 (2019) 1755.

[12]. Makoto I. Kobayashi, Maurizio Angelone, Sachiko Yoshihashi, Kunihiro Ogawa, Mitsutaka Isobe, Takeo Nishitani, Siriyaporn Sangaroon, Shuji Kamio, Yutaka Fujiwara, Tomomi Tsubouchi, Akira Uritani, Minoru Sakama, Masaki Osakabe, and the LHD Experiment Group, Thermal neutron measurement by single crystal CVD diamond detector applied with the pulse shape discrimination during deuterium plasma experiment in LHD, Fusion Eng. Des., 161 (2020) 112063.

[13]. P. Kavrigin, P. Finocchiaro, E. Griesmayer, E. Jericha, A. Pappalardo, C. Weiss, Pulse-shape analysis for gamma background rejection in thermalneutron radiation using CVD diamond detectors, Nucl. Instrum. Methods Phys. Res. A, 795 (2015) 88-91.

[14]. T. Williams, C. N'Diaye, D. Breton, K. Cassou, K. Dupraz, P. Favier, D. Jehanno, V. Kubytskyi, X. Liu, J. Maalmi, A. Martens, Y. Peinaud, A. Stocchi, F. Zomer, E. Griesmayer, P. Kavrigin, M.W. Ahmed, M. Sikora, H.R. Weller, Operation of a fast diamond γ-ray detector at the HIγS facility, Nucl. Instrum. Methods Phys. Res. A, 830 (2016) 391-396.

[15]. R.B. Firestone, Table of Isotopes 8th edn (New York: Wiley), 1996.

[16]. https://cividec.at

[17]. K. Ogawa, M. Isobe, T. Nishitani, T. Kobuchi, The large helical device vertical neutron camera operating in the MHz counting rate range, Rev. Sci. Instrum., 89 (2018) 113509.

[18]. T. Sato et al., Features of Particle and Heavy Ion Transport code System (PHITS) version 3.02, J. Nucl. Sci. Technol., 55 (2018) 684-690.

Figure captions

Table 1 The summary of the detection efficiencies of tritons and alpha particles in Cases I and II measured by the experiment and estimated by PHITS. The detection efficiencies are evaluated here as a ratio of the number of pulse signals to the number of neutrons injected into the SCD (4.5 mm × 4.5 mm). The errors in the measurement were evaluated as 1σ of the count numbers of tritons and alpha particles. The statistic errors in the count rate in PHITS results are also displayed in this figure.

Fig. 1 The definitions of Q_{fast} and Q_{total} in this work in a pulse by an alpha particle from ^{241}Am.

Fig. 2 The PSD results for alpha particles from ^{241}Am and gamma-rays from ^{60}Co. The count rates and total numbers of pulses for alpha particles and gamma-rays in this figure were 19 cps and 30 cps, and ~24000 (measurement for 1200s) and ~110000 (measurement for 3600 s), respectively.

Fig. 3 The schematic drawing of the SDD used in this work. The thermal neutron beam directions in Cases I and II are also presented.

Fig. 4 The results of PSD applied for about 53000 pulse data (event rate ~ 98 s^{-1}) obtained by the thermal neutron irradiation for 9 min in Case I

Fig. 5 The transport behaviors of (a) thermal neutrons and (b) energetic tritons generated in the ^{6}LiF in the SDD in Case I estimated by PHITS

Fig. 6 The histograms of (a) Q_{total} obtained in Case I (the same data set as presented in Fig. 4) and (b) energy deposition events estimated by PHITS for all pulse data, energetic tritons and alpha particles.

Table 1 M.I. Kobayashi et al.

Neutron beam direction	**Energetic ion**	**Count/neutron in experiment**	**Count/neutron in PHITS**	**C/E**
Case I	Alpha particles	$(3.80 \pm 0.04) \times 10^{-4}$	$(4.97 \pm 0.03) \times 10^{-4}$	1.31 ± 0.01
	Tritons	$(1.05 \pm 0.06) \times 10^{-3}$	$(1.06 \pm 0.05) \times 10^{-3}$	1.01 ± 0.01
Case II	Alpha particles	$(2.80 \pm 0.03) \times 10^{-4}$	$(3.86 \pm 0.04) \times 10^{-4}$	1.38 ± 0.02
	Tritons	$(7.51 \pm 0.05) \times 10^{-4}$	$(8.20 \pm 0.06) \times 10^{-3}$	1.09 ± 0.01

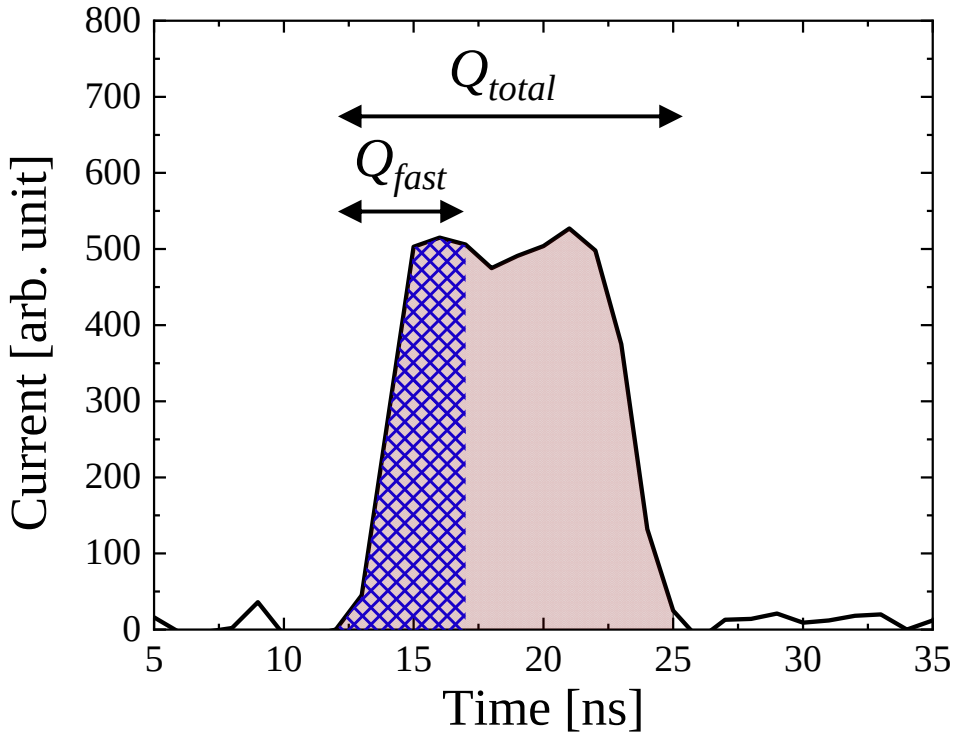

Fig. 1 M.I. Kobayashi et al.

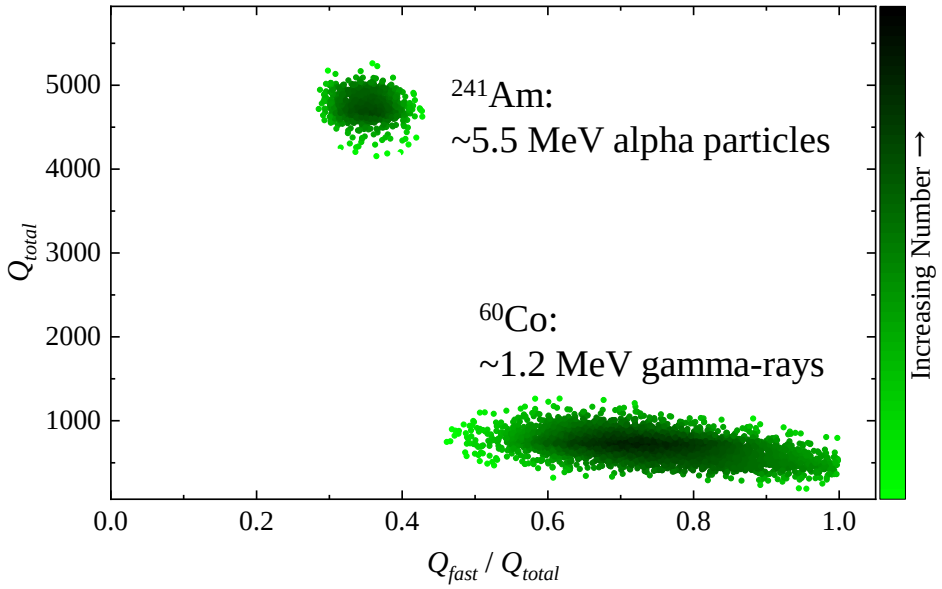

Fig. 2 M.I. Kobayashi et al.

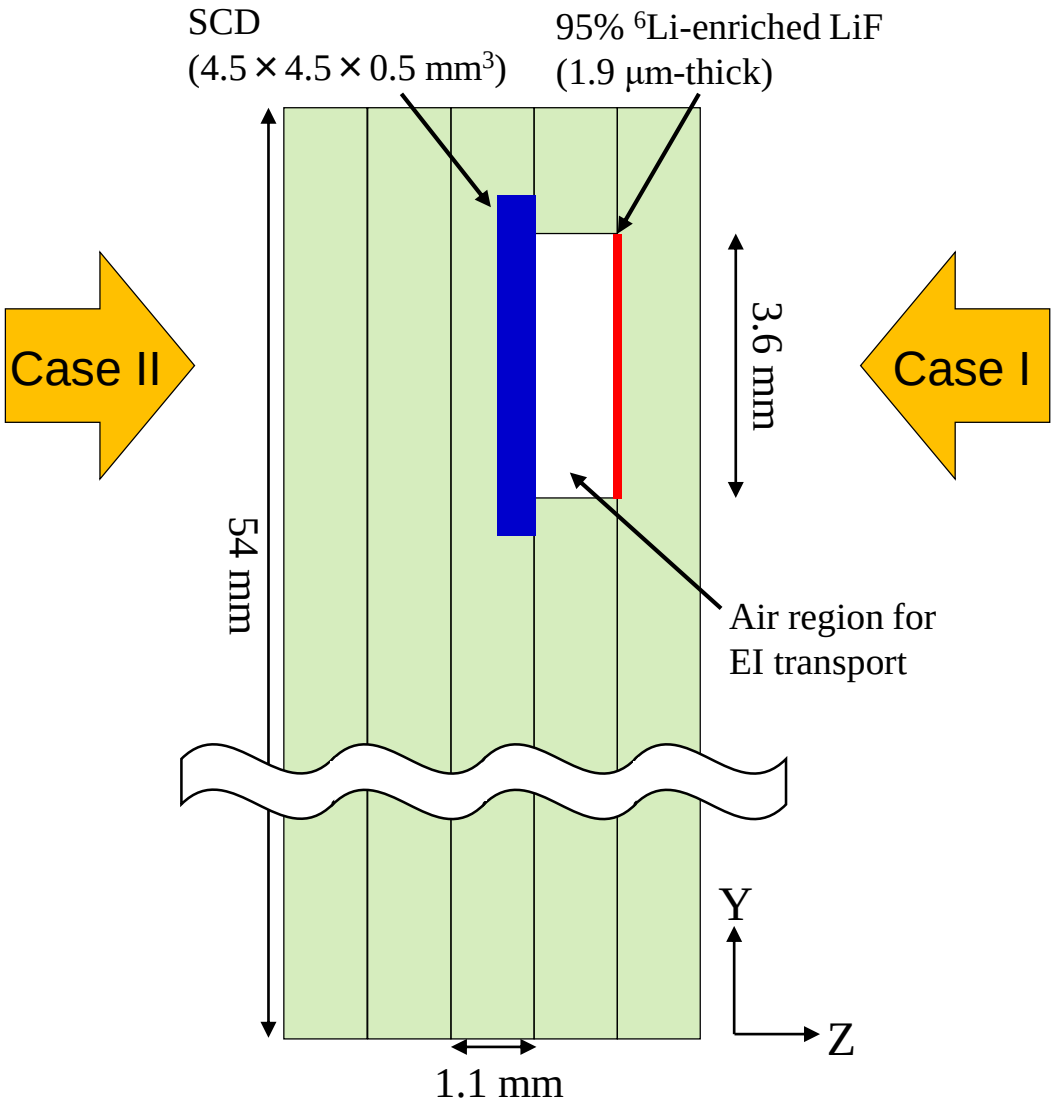

Fig. 3 M.I. Kobayashi et al.

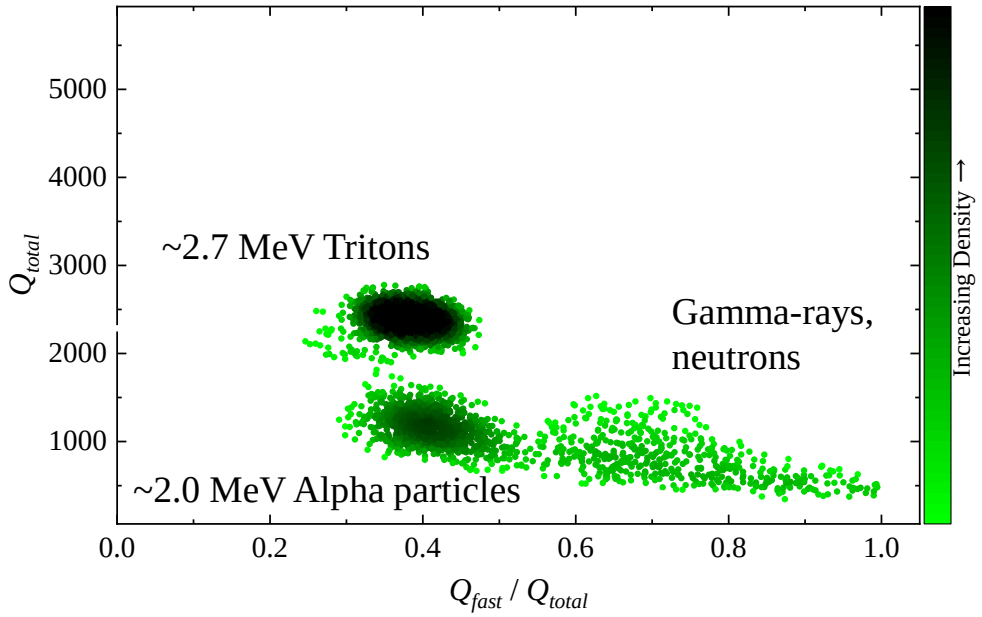

Fig. 4 M.I. Kobayashi et al.

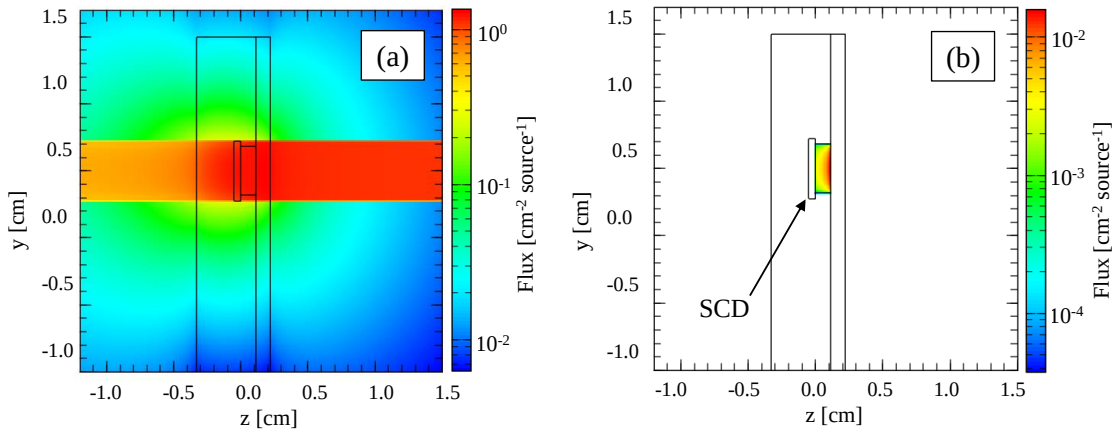

Fig. 5 M.I. Kobayashi et al.

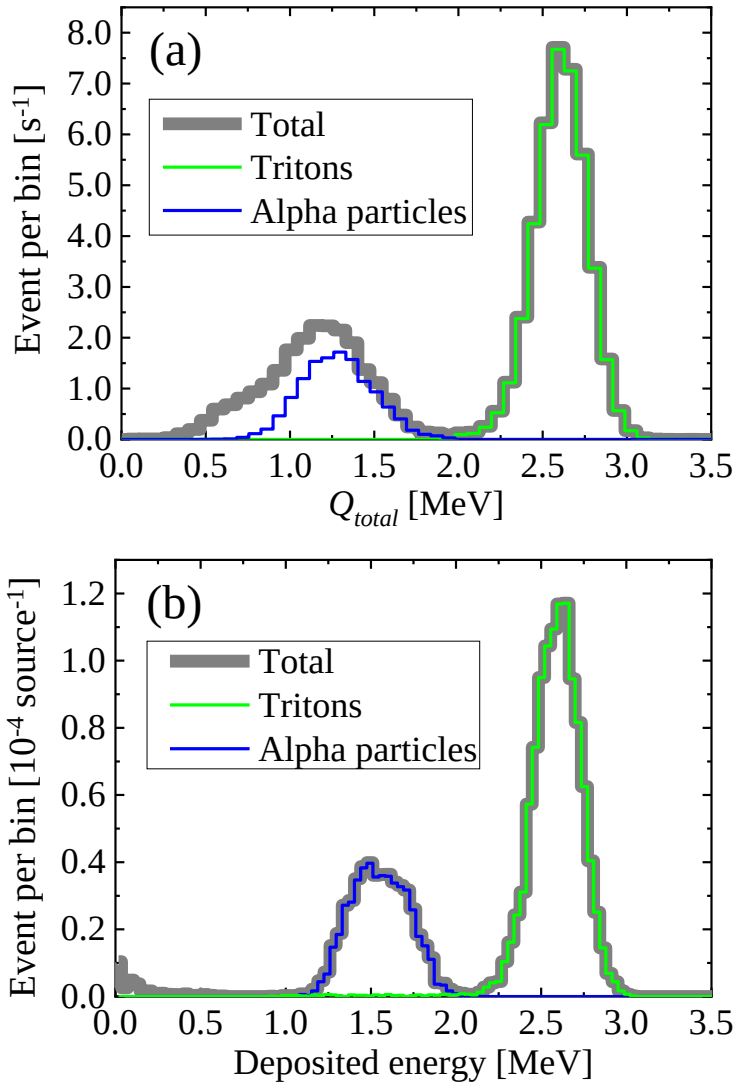

Fig. 6 M.I. Kobayashi et al.